Cell Reports

Article

Ribosome 18S m^{6}A Methyltransferase METTL5 Promotes Translation Initiation and Breast Cancer Cell Growth

Graphical Abstract

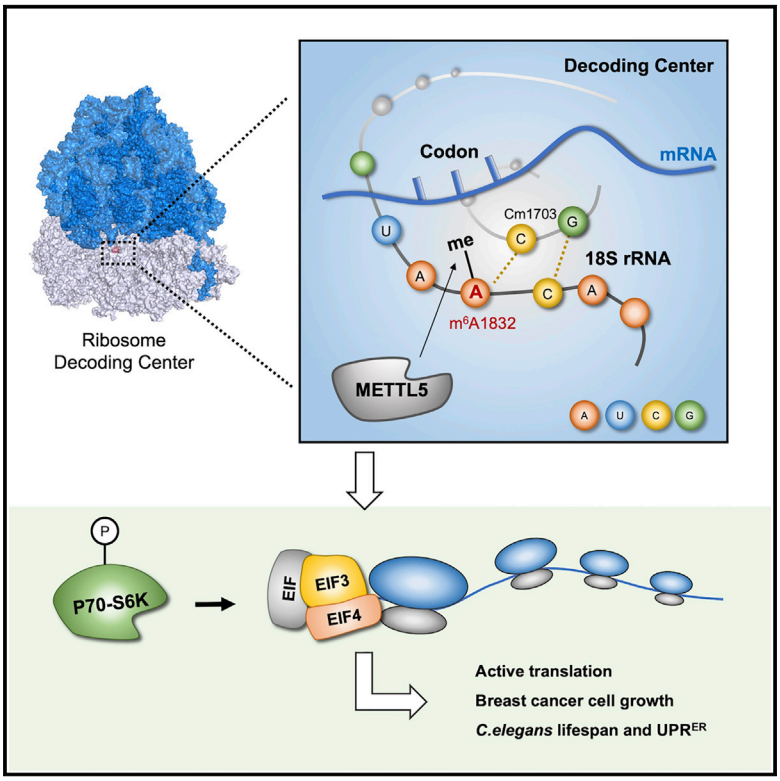

Highlights

- METTL5 shows strong substrate preference to 18S rRNA m^{6}A1832 motif UAACA
- The m^{6}A1832 modification may affect decoding center in favoring mRNA binding
- METTL5 promotes translation initiation, S6K activation, and breast cancer cell growth
- *C. elegans* METL-5 regulates stress response, lifespan, and UPR^{ER}

Authors

Bowen Rong, Qian Zhang, Jinkai Wan, ..., Honghui Ma, Ye Tian, Fei Lan

Correspondence

honghuima@tongji.edu.cn (H.M.), ytian@genetics.ac.cn (Y.T.), fei_lan@fudan.edu.cn (F.L.)

In Brief

Rong et al. show that the conserved 18S rRNA m^{6}A methyltransferase has strong substrate preference and regulates translation initiation. METTL5-mediated m^{6}A1832 may fine-tune decoding center conformation in favoring mRNA interaction. METTL5 expression is elevated in breast cancer tissue and is required for breast cancer cell growth.

Rong et al., 2020, Cell Reports *33*, 108544
December 22, 2020
https://doi.org/10.1016/j.celrep.2020.108544

CellPress

Cell Reports

CellPress
OPEN ACCESS

Article

Ribosome 18S m^{6}A Methyltransferase METTL5 Promotes Translation Initiation and Breast Cancer Cell Growth

Bowen Rong,[1,7] Qian Zhang,[2,3,7] Jinkai Wan,[1] Shenghui Xing,[1] Ruofei Dai,[1] Yuan Li,[4] Jiabin Cai,[1] Jiaying Xie,[1] Yang Song,[1] Jiawei Chen,[5] Lei Zhang,[1] Guoquan Yan,[1] Wen Zhang,[1] Hai Gao,[1] Jing-Dong J. Han,[5] Qianhui Qu,[1] Honghui Ma,[6,*] Ye Tian,[2,3,*] and Fei Lan[1,8,*]

[1]Shanghai Key Laboratory of Medical Epigenetics, State International Co-laboratory of Medical Epigenetics and Metabolism, Institutes of Biomedical Sciences, Fudan University, and Key Laboratory of Carcinogenesis and Cancer Invasion, Ministry of Education, Liver Cancer Institute, Zhongshan Hospital, Fudan University, Shanghai 200032, China

[2]State Key Laboratory of Molecular Developmental Biology, Institute of Genetics and Developmental Biology, Chinese Academy of Sciences, Beijing 100101, China

[3]University of Chinese Academy of Sciences, Beijing 100093, China

[4]Department of Pathology, Fudan University Shanghai Cancer Center, Shanghai 200032, China

[5]Peking-Tsinghua Center for Life Sciences, Academy for Advanced Interdisciplinary Studies, Center for Quantitative Biology (CQB), Peking University, Beijing 100871, China

[6]Key Laboratory of Arrhythmias of the Ministry of Education of China, East Hospital, Tongji University School of Medicine, Shanghai 200120, China

[7]These authors contributed equally

[8]Lead Contact

*Correspondence: honghuima@tongji.edu.cn (H.M.), ytian@genetics.ac.cn (Y.T.), fei_lan@fudan.edu.cn (F.L.)

https://doi.org/10.1016/j.celrep.2020.108544

SUMMARY

N6 methylation at adenosine 1832 (m^{6}A1832) of mammalian 18S rRNA, occupying a critical position within the decoding center, is modified by a conserved methyltransferase, METTL5. Here, we find that METTL5 shows strong substrate preference toward the 18S A1832 motif but not the other reported m^{6}A motifs. Comparison with a yeast ribosome structural model unmodified at this site indicates that the modification may facilitate mRNA binding by inducing conformation changes in the mammalian ribosomal decoding center. METTL5 promotes p70-S6K activation and proper translation initiation, and the loss of METTL5 significantly reduces the abundance of polysome. METTL5 expression is elevated in breast cancer patient samples and is required for growth of several breast cancer cell lines. We further find that *Caenorhabditis elegans* lacking the homolog *metl-5* develop phenotypes known to be associated with impaired translation. Altogether, our findings uncover critical and conserved roles of METTL5 in the regulation of translation.

INTRODUCTION

Mammalian ribosome is composed of two functional components, the small subunit (40S) and the large subunit (60S), including nearly 80 ribosomal proteins (RPs) and four ribosomal RNAs (rRNAs), which are orchestrated by translation factors and transfer RNAs (tRNAs) to control the fidelity and rate of translation. A variety of chemical modifications have been found in rRNAs from prokaryotes to eukaryotes, such as methylation or acetylation in both the nucleotide bases and the ribose moieties. The total number of rRNA modifications expands significantly with evolution, and currently more than 130 rRNA modifications are identified in humans (Natchiar et al., 2017). Some modifications with essential roles are conserved throughout kingdoms, such as Cm1703, m$_2$^{6}A1850, and m$_2$^{6}A1851 on 18S rRNA, which are required for stability or maturation of ribosomes (Zorbas et al, 2015; Kimura and Suzuki, 2010; Poldermans et al., 1979; Xu et al., 2008). However, some other modifications appear only in certain organisms. For instance, Ψ1056 and m^{7}G1639 of 18S rRNA are conserved from yeasts to humans but are absent in prokaryotes. The m^{6}A modification of 18S rRNA was initially reported in *Xenopus laevis* (A1789) and human (A1832) (Choi and Busch, 1978; Maden, 1986), and recently in *C. elegans* (A1717) (Liberman et al., 2020) as well as other metazoans and archaea (Chen et al., 2020; Coureux et al., 2020; Ignatova et al., 2020; Leismann et al., 2020; Natchiar et al., 2017; Nürenberg-Goloub et al., 2020; van Tran et al., 2019; Xing et al., 2020), but was not identified in prokaryotes and yeasts (Sergiev et al., 2018). On the basis of these observations, it is plausible that certain regulatory functions, rather than housekeeping roles, may be carried by these variable modifications to alter cellular translation activities, in response to capricious environmental pressures.

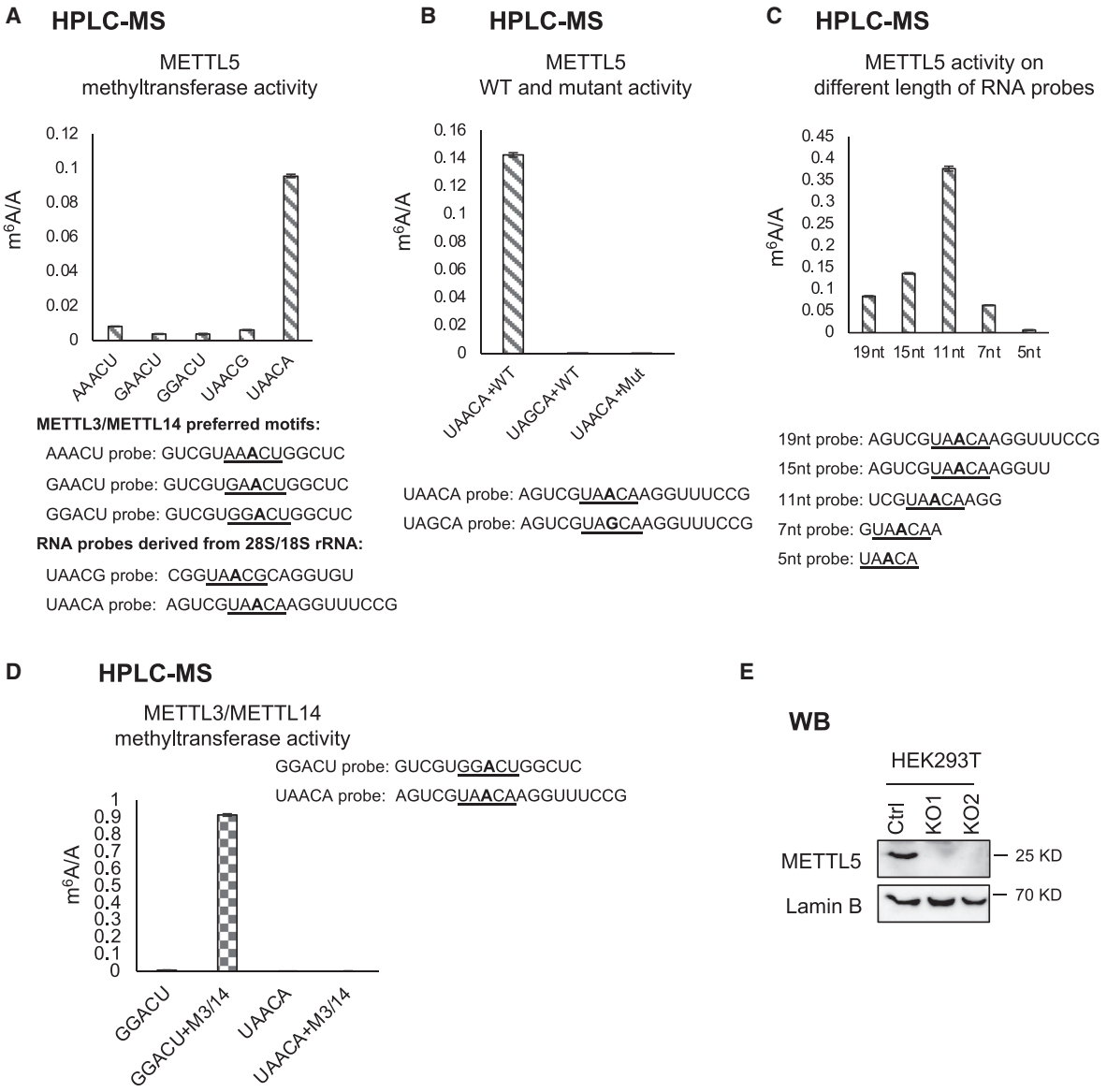

(legend on next page)

Known as one of the most abundant modifications in mRNA, small nuclear RNA (snRNA) U6, and rRNA, m^6A modifications are introduced to N6 adenosine at specific positions by a group of RNA methyltransferases containing a (D/N) PP (F/Y) motif. For example, METTL3-mediated m^6A in mRNA and non-coding RNA is involved in regulating RNA splicing, stability, and translation (Shi et al., 2019), while METTL16-mediated snRNA U6 m^6A fine-tunes U6 activity toward select substrate introns during splicing (Doxtader et al., 2018; Pendleton et al., 2017). For rRNAs, m^6A modification was found at the 18S A1832 and 28S A4220 sites in humans (Natchiar et al., 2017). The 28S m^6A4220 is catalyzed by ZCCHC4 and required for effective translation and cell proliferation (Ma et al., 2019; van Tran et al., 2019). Recently, several groups have demonstrated that METTL5 mediates the modification in HCT116 cells, HAP1 cells (a human induced pluripotent stem cell line), mouse embryonic stem cells (mESCs), *C. elegans*, and *Drosophila* and is active on purified full-length 18S RNA substrates or synthesized RNA oligos (Chen et al., 2020; Ignatova et al., 2020; Leismann et al., 2020; Liberman et al., 2020; van Tran et al., 2019; Xing et al., 2020). However, the substrate requirement and specificity of METTL5 and its biological function remain to be elucidated. METTL5 orthologs can be found in worms, flies, and vertebrates, but not in yeasts, implying a potential function in orchestrating multicellular growth. However, METTL5 ortholog and the corresponding 16S m^6A1469 also exist in archaea (Coureux et al., 2020; Nürenberg-Goloub et al., 2020), unicellular organisms that live in extreme conditions, suggesting the regulation may be connected to stress responses. *METTL5* mutation was recently reported to cause autosomal-recessive intellectual disability and microcephaly in two large families of Pakistani and Yemenite origins (Richard et al., 2019). Altogether, these findings suggest that METTL5 may play important roles in regulating ribosome function and development, possibly through 18S m^6A1832 modification.

Here, we report that METTL5 is capable of catalyzing m^6A on RNA substrates specifically containing the UAACA motif derived from 18S A1832 but is inert toward the RRACH and UAACG motifs preferred by METTL3 and ZCCHC4 *in vitro*. Analysis of available high-resolution ribosome structures reveals that this modification is placed in a critical position of the decoding center and potentially favors a conformation forming strong interaction with mRNA undergoing active translation. HEK293T cells lacking METTL5 completely lost m^6A1832, displayed impaired process from 80S ribosomes onward to polysomes, and showed significant reduced global translation and S6K activation. METTL5 is elevated in breast cancer samples and is required for proper growth of several breast cancer cell lines. Loss of METTL5 led to increased apoptosis and cell-cycle arrest in these cancer cell lines. Furthermore, we showed that the worm *metl-5* mutants displayed significantly increased thermotolerance and lifespan and a strongly enhanced UPR^{ER}. Our data thus reveal an evolutionary conserved function of METTL5 in catalyzing 18S m^6A modification and regulating protein translation, which control human cell growth and worm stress response and lifespan.

RESULTS

METTL5 Specifically Mediates 18S rRNA m^6A1832 Both *In Vitro* and in Cells

Among the METTL family of proteins, METTL5 has been understudied until very recently. METTL5 contains a typical SAM-binding GxGxG motif and a conserved m^6A-catalyzing NPPF motif, and it has been recently demonstrated as the methyltransferase of the m^6A1832 of 18S rRNA in multiple species (Chen et al., 2020; Ignatova et al., 2020; Leismann et al., 2020; Liberman et al., 2020; van Tran et al., 2019; Xing et al., 2020). In order to characterize METTL5 substrate specificity, we purified recombinant wild-type and catalytic mutant METTL5 from SF9 insect cells using a baculoviral expressing system and set up an *in vitro* RNA methylation assay using various substrate RNA probes containing motifs derived from different RNA species. After high-performance liquid chromatography-mass spectrometry (HPLC-MS) analyses, we found that METTL5 showed specific activities toward the UAACA motif, which is derived from 18S rRNA A1832 site, but not the 28S rRNA m^6A motif UAACG containing the A4220 site and the METTL3/METTL14-preferred substrate motif RRACH (where R = A or G and H = A, C, or U) (Figure 1A). Such activity was dependent on the intact NPPF motif, as the mutant METTL5 showed no activity under the same assay conditions (Figure 1B). Furthermore, when we mutated the center A to G (UAACA to UAGCA) in the RNA substrate, no m^6A activity could be detected (Figure 1B). We next investigated the requirement of the flanking sequences to the METTL5-mediated m^6A catalysis, using synthetic RNA probes ranging from 5 to 19 nt. We found that the 7 nt probe was enough to show detectable activity, while the 11 nt probe displayed the strongest activity for unknown reason (Figure 1C).

Figure 1. METTL5 Specifically Methylates 18S rRNA *In Vitro* and in HEK293T Cells

(A) Methyltransferase assay of recombinant wild-type (WT) METTL5 toward RNA probes containing the indicated 5 nt motifs. Data are presented as mean ± SD. The potential methylated adenosines are in the center.

(B) Methyltransferase assay of recombinant WT and catalytic mutant (Mut) METTL5 toward the indicated probes. Data are presented as mean ± SD.

(C) Methyltransferase assay of recombinant METTL5 on UAACA-containing probes with indicated lengths derived from 18S sequence. Data are presented as mean ± SD.

(D) Comparison of the enzymatic activities of the recombinant METTL3/METTL14 (M3/14) complex on RNA probes containing GGACU and UAACA motifs. Data are presented as mean ± SD.

(E) Western blot examination of METTL5 protein levels in the parental (Ctrl) and two independent METTL5 knockout lines (KO1 and KO2) of HEK293T cells.

(F) HPLC-MS analyses showing m^6A/G levels of total RNA, polyA RNA, 28S rRNA, and 18S rRNA fractions. Note that, m_2^6A/G levels were measured only in 18S rRNA. Data are presented as mean ± SD; $^{**}p < 0.01$.

Note that all experiments were repeated more than three times, and one replicate is shown.

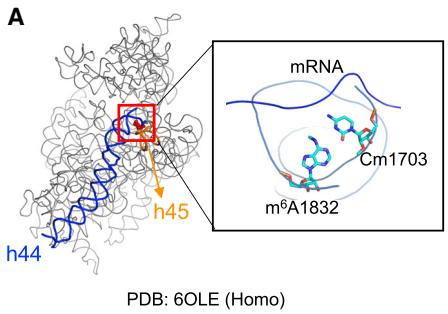

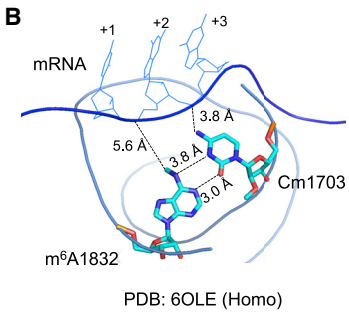

Figure 2. 18S rRNA m^{6}A1832 Occupies the Decoding Center and Potentially Forms Interaction with the Translating mRNA

(A) Structural view of the conformations of 18S rRNA helix 44 (blue) and helix 45 (orange) and positions of m^{6}A1832 and Cm1703 in the human ribosome structure (PDB: 6OLE).

(B–D) The spatial positions of m^{6}A1832-Cm1703, A1763-Cm1639, and A1500-m^{4}Cm1402 pairs, in *Homo sapiens* (B), yeast (C), and *E. coli* (D) decoding centers. The non-classical base pairings between the indicated bases and the distances from the indicated atoms to the mRNA backbone phosphates were measured (PDB: 6OLE, 6T7T, and 5AFI).

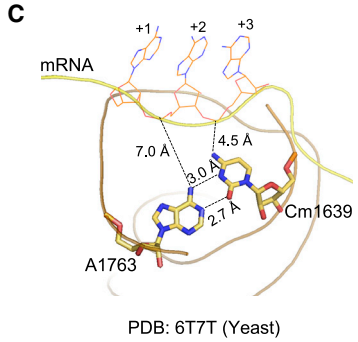

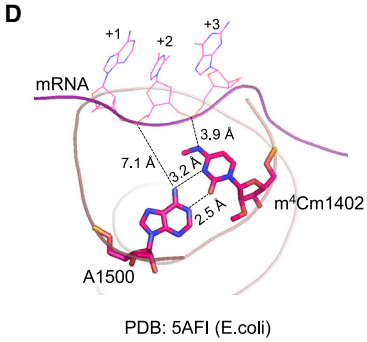

Of note, the 18S UAACA motif is also a much less preferred substrate for the METTL3/METTL14 complex (Figure 1D).

Consistent with the *in vitro* results and recent reports (Chen et al., 2020; Ignatova et al., 2020; Leismann et al., 2020; Liberman et al., 2020; van Tran et al., 2019; Xing et al., 2020), METTL5 knockout (KO) in HEK293T cells led to the complete loss of 18S rRNA m^{6}A1832, without detectable alterations of m^{6}A abundance in the total mRNA species and 28S rRNA (Figures 1E and 1F). To examine whether METTL5 could be responsible for the m^{6}A modification of a minority of mRNA molecules, we searched a published dataset of single-nucleotide mapping of mRNA m^{6}A for the 7 nt core motif, GUAACAA, and identified only four GUAm^{6}ACAA sites in *ZNF629*, *SON*, *SHOC*, and *STT3B* transcripts (Linder et al., 2015). Further m^{6}A RNA immunoprecipitation (IP) and qPCR analyses found that none of the four sites were affected by loss of METTL5, suggesting that METTL5 is likely a specific m^{6}A methyltransferase for 18S rRNA but not mRNA (Figure S1A; Table S1). This hypothesis is also supported by the observation of a predominant nucleoli localization of METTL5 in a substantial cell population, although moderate cytoplasmic localization was also observed in a subset of cells (Figure S1B). We also observed a reduction of m^{6}A in the total RNA fraction, which was likely due to the abundance of 18S rRNA counting for approximately 30% of the total cellular RNA mass (Figure 1F). In addition, A1832 is close to the 3′ end of 18S rRNA (1,869 nt in total) and is 18–19 nt prior to another two conserved modifications, m$_2$^{6}A1850 and m$_2$^{6}A1851, which were unaffected by the absence of METTL5, indicating that these latter two modifications are independent of METTL5 (Figure 1F).

The above findings are consistent with several recent published studies (Chen et al., 2020; Ignatova et al., 2020; Leismann et al., 2020; Liberman et al., 2020; van Tran et al., 2019; Xing et al., 2020). Here we further provided proof that METTL5 could specifically methylate m^{6}A1832 with strong sequence specificity toward UAACA motif, which is a much less preferred substrate for METTL3 and ZCCHC4 (Ma et al., 2019; Zhang et al., 2019). Our results indicate that the substrate primary sequence of 7 nt is enough for the *in vitro* reconstitution of METTL5 activity, and the substrate specificity is intrinsically built into the m^{6}A enzymes, which indicates the possibilities of differential regulation.

m^{6}A1832 Modification May Fine-Tune the Interaction between Ribosome Decoding Center and Translating mRNA

A1832 is located at the 18S rRNA h44 loop, an important structural component together with the h45 loop to form the decoding center in the human ribosome small subunit (Figure 2A). Interestingly, m^{6}A1832 modification is in close spatial vicinity to the other known h44-h45 modifications, including Cm1703, m^{3}U1830, m$_2$^{6}A1850, and m$_2$^{6}A1851, despite the distant primary sequence registry. Of note, m^{6}A1832 forms non-classical base pairing with Cm1703, which is close to the translating mRNA (Figure 2B). Such non-classical base-pairing events have also been observed in yeast and *E. coli*, even though the corresponding A1763 and A1500 sites are not modified by m^{6}A in yeast and *E. coli*, respectively (Figures 2C and 2D). Association between the corresponding unmodified A1500 and m^{4}Cm1402 in *E. coli* was believed to stabilize the mRNA in the decoding center (Kimura and Suzuki, 2010). Notably, m$_2$^{6}A1850 and m$_2$^{6}A1851 were also reported to play critical roles in maintaining proper spatial conformation of the decoding center (Demirci et al., 2010; Poldermans et al., 1979). These studies suggest that the modification status of A1832 may influence the conformation of the ribosomal decoding center.

In order to probe the possible role of the m^{6}A1832 modification, we extensively screened the available ribosome structures with resolution greater than 3.5 Å to discriminate the modification

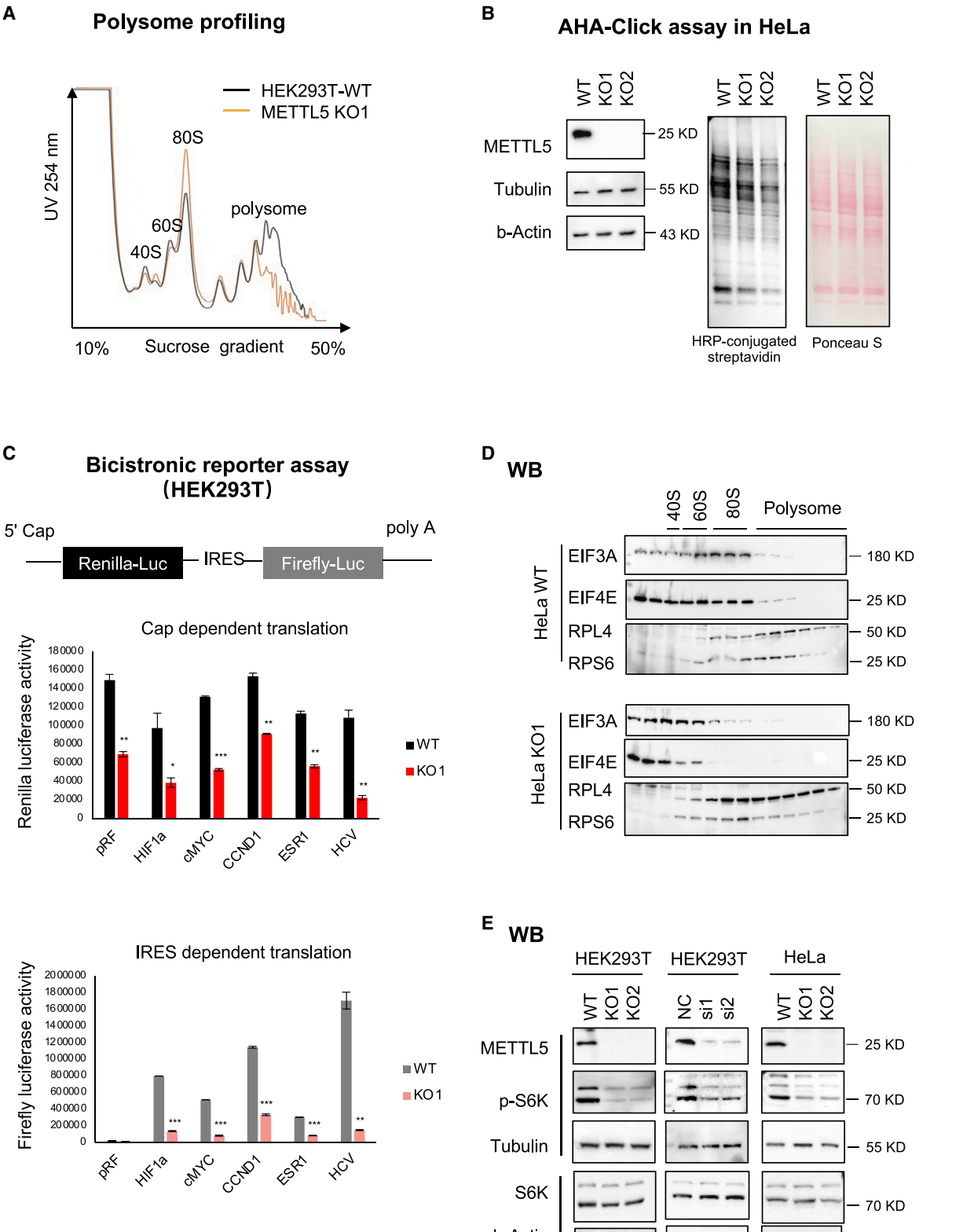

(legend on next page)

status of the A1832 site. Among them, six human and rabbit ribosome structures (PDB: 6OLE, 4UG0, 6QZP, 6SGC, 5LZS, and 5AJ0) (Behrmann et al., 2015; Chandrasekaran et al., 2019; Khatter et al., 2015; Li et al., 2019; Natchiar et al., 2017; Shao et al., 2016) showed unambiguous density for the N6 methyl group of m^6A1832 (Figures S2A–S2E), although only in 6OLE was the N6 methyl group modeled. No human or rabbit ribosome structure with sufficient density quality to represent the unmodified state of A1832 was found. Therefore a yeast ribosome structure (PDB: 6T7T) with mRNA (Figure S2F) (Tesina et al., 2020) and unmodified A1763, corresponding to human A1832, was used for the comparison with 6OLE, which contains both mRNA and the modified m^6A1832 18S rRNA.

The overall conformations of the h44 loops and decoding centers are similar in yeast and human (Figure S2G), and the non-classical base pairs of A1763-Cm1639 and m^6A1832-Cm1732 are underneath the mRNA backbones, with the N6 adenosines and N4 cytosines pointing to the main-chain +2 and +3 phosphates of the P-site codons (Figures 2B, 2C, and S2H). However, close examination revealed several differences. First, a small but significant movement of the human m^6A1832 toward the P-site codon +2 phosphate compared with yeast A1763 was observed. Such movement places the human N6 methyl group of A1832 5.6 Å away from mRNA, shorter than the yeast unmodified A1763 (7.0 Å). Second, contrary to the tight association within the yeast A1763-Cm1639 duo, the distance between the human m^6A1832 and Cm1703 is slightly increased, indicating weakened base pairing in the human structure (Figures 2B and 2C). This effect could be due to reduced hydrogen bond formation between the m^6A1832 and the Cm1703, as the methyl group replaces one bonding hydrogen at the N6 site of A1832 (Figure 2B). Interestingly, such weakened base pairing of m^6A1832-Cm1703 may allow Cm1703 to move closer to the mRNA codon +3 phosphate (Figures 2B and 2C; 3.8 Å in human versus 4.5 Å in yeast), which potentially creates a stronger hydrogen bond with mRNA compared with that in the yeast ribosome.

We also made further comparisons with the *E. coli* ribosome (PDB: 5AFI) (Fischer et al., 2015), which does not have the m^6A modification at the A1500 site but has the m^4Cm1402 instead (Figure 2D). The distance between the two paired bases in the *E. coli* structure is similar to that in the yeast structure, and the unmodified *E. coli* A1500 is 7.1 Å away from the mRNA backbone (codon +2 phosphate), similar to that in the yeast structure. However, the distance between the N4 m^4Cm1402 and mRNA (codon +3 phosphate) is 3.9 Å, close to that in the human structure.

It is unclear whether these modifications directly induce such spatial differences, but in the human structure, with m^6A at A1832, non-classical base pairing between the two critical bases is weakened, and the distances of mRNA and the two bases are in general closer than those in the yeast and *E. coli* ribosome structures. Such observations prompted us to hypothesize that the m^6A modification of A1832 may play a role in fine-tuning ribosome activity by shaping the decoding center in favoring a mRNA-bound conformation.

Loss of METTL5 Led to Reduced Polysome Fraction, Accumulated 80S Ribosomes, and Attenuated Global Translation

To validate whether loss of the m^6A1832 modification could lead to alterations of ribosome function and polysome profile, we performed sucrose gradient analyses of polysome profile. In the analyses, we observed a significant decrease in the polysome portion in the METTL5-KO cells, which is the most active translation fraction of ribosomes (Figure 3A).

Compared with the ribosomes isolated from the parental HEK293T cells, the ribosomes from METTL5-KO cells showed an accumulation of the 80S fraction (Figure 3A). These findings indicated that the subunit joining to form the 80S ribosomes was largely unaffected in the METTL5-KO cells, but much fewer 80S ribosomes were able to proceed onward to the polysome fraction for active translation. We then used azidohomoalanine (AHA), a methionine analog that contains an azide moiety allowing biotin labeling through a click-chemistry reaction, to detect the newly synthesized proteins in cells. In support of the above notion, we observed a significantly reduced global translation in the METTL5-KO HeLa cells compared with the parental control cells (Figure 3B). We further measured protein content in the equal numbers of the control and METTL5-KO HeLa cells and found that the METTL5-KO cells contained ~30% fewer proteins compared with the parental control cells (Figure S3A).

To reaffirm the AHA results, we used several widely used bicistronic reporters to investigate the 5′ cap- and various internal ribosomal entry site (IRES)-dependent translation efficiencies. We found that both the 5′ cap- and IRES-dependent translation were significantly reduced in the METTL5-KO HEK293T cells compared with the parental control cells (Figure 3C).

Loss of METTL5 Led to Reduced 80S-Associated Initiation Factors and Attenuated S6K Activation

On the basis of the above results, we hypothesized that the defect of 80S ribosomes proceeding to polysomes in METTL5-KO cells may be due to impaired initiation of translation. The translation initiation process is known to be controlled by ribosome-associated initiation factors (EIFs), which bridge the mRNA recognition and ribosome loading. In order to test the idea, we examined EIFs, such as the EIF3 and EIF4 components. Interestingly, we observed significantly shifted patterns of EIF3A

Figure 3. Loss of METTL5 Led to Reduced Polysome Fraction and Attenuated Global Translation

(A) Polysome profiling by sucrose density gradient showing decreased polysomes and accumulated 80S monosomes.

(B) AHA-Click labeling assay showing the newly synthesized proteins in the indicated cells.

(C) Luciferase reporter assays showing that METTL5 knockout reduced the activity of both IRES-dependent and 5′ cap-dependent translation activities, indicated by the Firefly and Renilla activities, respectively. Data are presented as mean ± SD; ***$p < 0.001$.

(D) Western blot analyses of the indicated proteins from individual fractions separated by polysome profiling in the control and KO HeLa cells.

(E) Western blot analysis showing reduced S6K phosphorylation level in METTL5-KO and siRNA-treated cells.

Note that all experiments were repeated more than three times, and one replicate is shown.

and EIF4E from 80S to smaller sizes (40S subunit), indicating that in METTL5-KO cells, the 80S ribosomes were associated with significantly less EIF3A and EIF4E (Figure 3D). As the EIF4 complex is critical for cap-dependent translation and EIF3 is involved in certain IRES-dependent translation, these results are in agreement with the observation of a globally reduced translation (Figures 3B and 3C).

Further interacting protein analysis by HA IP-MS/MS using HA-METTL5 as the bait found that HA-METTL5 interacted with many ribosomal proteins and translation initiation/elongation factors (including EIF3s/EIF4s/EEFs), as well as the previously reported TRMT112 (Figures S3B and S3C) (Chen et al., 2020; Ignatova et al., 2020; Leismann et al., 2020; van Tran et al., 2019). These results indicate that METTL5 is a component of a large protein complexes containing EIFs and RPs. Therefore, EIF dissociation from 80S ribosome could also be a consequence of the loss of METTL5 protein through a protein-protein interacting mechanism.

In parallel to the EIF regulation, the S6K (also known as p70-S6K or RPS6 kinase) activation by T389 phosphorylation is also a critical upstream signal for the translation initiation, which is under the regulation of AMPK and mTOR signaling pathways to adjust protein homeostasis upon the environmental changes. To further test the hypothesis of an initiation defect of ribosomes upon loss of METTL5, we examined S6K phosphorylation levels in the control and METTL5-KO-treated or small interfering RNA (siRNA)-treated HEK293T and HeLa cells. In both cell lines, we found that the S6K phosphorylation levels were significantly reduced with METTL5 loss, further supporting the idea that METTL5 was required for proper translation initiation (Figure 3E).

Taken together, we concluded that the ribosomes in METTL5-KO cells showed an attenuated translation initiation activity, as evidenced by less EIF association with the 80S ribosome and reduced S6K activation, consistent with the observation of global reduction of translation in METTL5-KO cells.

METTL5 Protein Is Elevated in Breast Cancer and Is Required for Optimal Growth of Breast Cancer Cell Lines

Protein translation activity is generally connected to cell growth and proliferation and is widely elevated in cancer to fulfill the demand of cancerous growth (Pelletier et al., 2018; Robichaud et al., 2019). The Cancer Genome Atlas (TCGA) analysis revealed METTL5 amplification events in breast cancer and several other types of cancers (Figure S4A, left). Although the overall METTL5 amplification frequency in breast cancer was low, it was the major form of the DNA level alterations, and almost no METTL5 deletion was detected in breast cancer (Figure S4A, left). Importantly, overall survival analysis using the publicly available kmplot database revealed a significant correlation of higher METTL5 expression level and poorer survival rates of breast cancer patients (Figure S4A, right) (Győrffy et al., 2010). To explore the connection of METTL5 to breast cancer, we collected 10 pairs of breast cancer tumor tissues and corresponding paratumor tissues as controls. We found that METTL5 protein levels were upregulated in 7 of the 10 paired tumor tissues compared with the paratumor tissues (Figure 4A). This observation indicated that METTL5 may be involved in breast cancer tumorigenesis.

We further examined METTL5 protein levels in a small panel of breast cancer cell lines (Figure 4B). We found that METTL5 protein levels were largely comparable among these cell lines, with the exception of ZR75-30, which had the lowest levels. Interestingly, ZR75-30 also showed the lowest levels of S6K phosphorylation (Figure 4B). As we found that METTL5 was required for proper S6K phosphorylation in HEK293T and HeLa cells (Figure 3E), these data suggest that METTL5 might be connected to cellular state, especially for growth. Therefore, we hypothesized that METTL5 loss may retard cancer cell growth. To test this, siRNAs were used to knock down METTL5 in four breast cancer cell lines over 3 days, followed by a second round of siRNA treatment, and the cell growth was then monitored for another three consecutive days. Growth in the METTL5 siRNA-treated cell lines was greatly diminished compared with the control cells (Figure 4C). Further analyses demonstrated that this reduced growth was concomitant with significantly elevated apoptosis in the METTL5-knockdown cell lines (Figure S4B). Although no cell cycle changes were observed in MCF7 cells, increased G2/M arrest was observed in the other three cell lines upon loss of METTL5 (Figure S4B). Importantly, we again observed significantly reduced S6K phosphorylation in these cancer cell lines with METTL5 deficiency (Figure 4D), consistent with our findings in HEK293T cell and HeLa cells. Interestingly, although HEK293T growth was perturbed by METTL5 loss, knockdown of METTL5 did not affect HeLa cell growth (Figure S4C), indicating that certain cell types, such as the previously reported HCT116, mESC, and HAP1 cells (Ignatova et al., 2020; Wang et al., 2020; van Tran et al., 2019), may bypass METTL5 regulation to maintain growth demand through a yet to be identified mechanism.

C. elegans METL-5 Mediates 18S m^6A and Regulates Stress Response, Lifespan, and UPR^{ER}

To uncover the function of METTL5 at the whole-organism level and to examine whether its regulation of translation is conserved in a different species, we chose *C. elegans*, in which translational defects are connected to known phenotypes, such as extended lifespan and increased stress responses (Hansen et al., 2007).

In *C. elegans*, *metl-5* is the homolog of *METTL5*, with a sequence similarity of 65% at the amino acid level and with 93.5% of the coding regions aligning with the human gene. Worms lacking *metl-5* were viable and did not display any obvious developmental defects (Figure S5A). To identify whether the function of METL-5 is conserved in *C. elegans*, we measured the m^6A modification of rRNAs in two *metl-5* deletion mutant strains. We found that the m^6A modification at A1717 (the corresponding position of human A1832) of 18S rRNA was strongly reduced in *metl-5* mutant worms, while the m^6A modification of 26S rRNA was not affected (Figure S5B). This indicates that the enzymatic activity of the METTL5 homolog METL-5 in *C. elegans* is evolutionarily conserved, consistent with a recent report (Liberman et al., 2020). Importantly, the *metl-5* mutant animals exhibited significantly longer lifespan and heat resistance compared with the control wild-type animals (Figures S5C–S5E). Of note, the enhanced stress tolerances of *metl-5* mutant animals were also recently reported by Liberman et al. (2020). As mentioned above, similar phenotypes, such as the extended

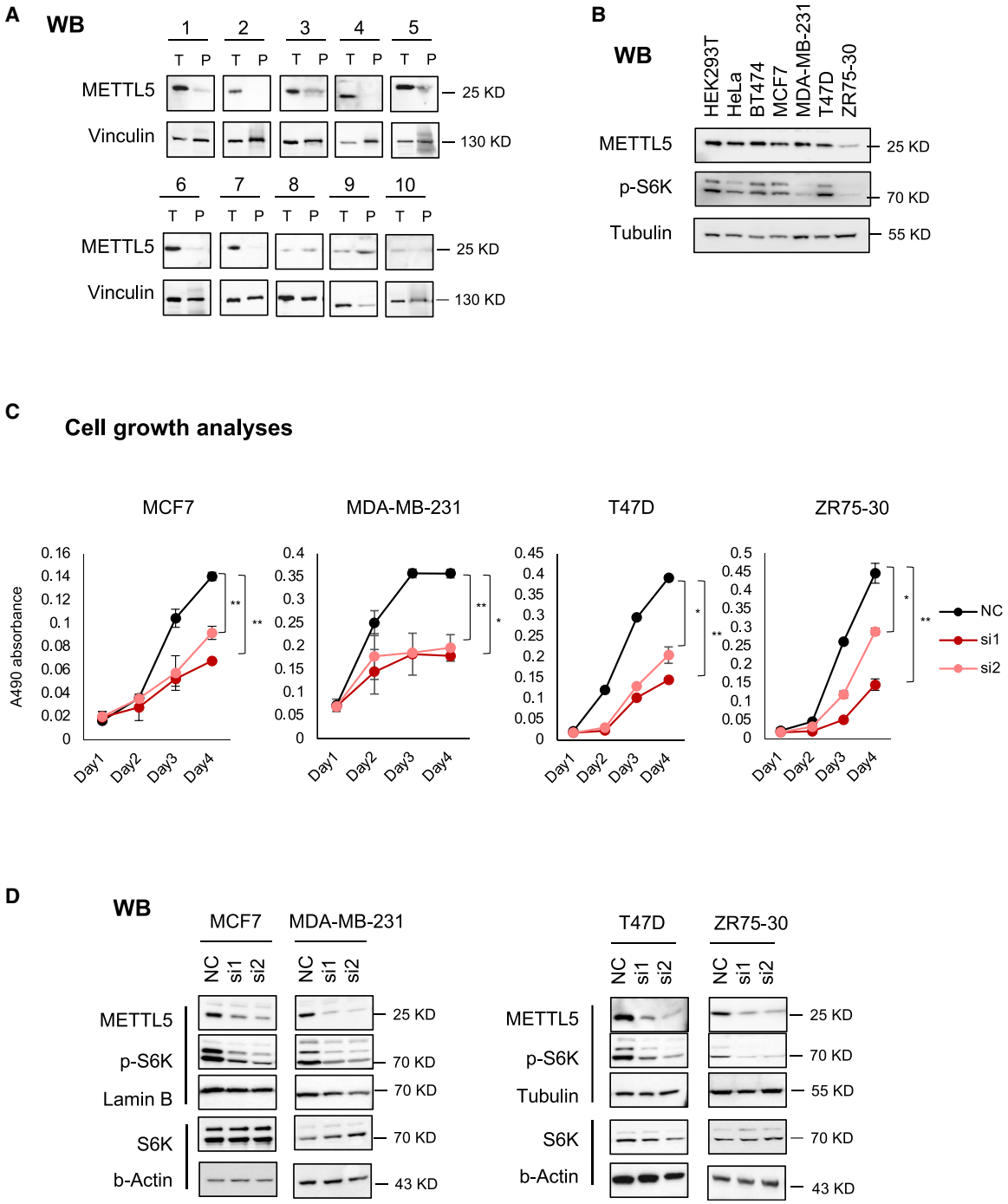

Figure 4. METTL5 Is Required for Growth and S6K Activation of Breast Cancer Cell Lines

(A) Western blot (WB) analyses showing METTL5 protein levels in paired breast tumor (T) and paratumor (P) samples from patients.

(B) WB analyses showing METTL5 protein and S6K phosphorylation (S6Kp) levels in the indicated breast cancer cell lines.

(C) Growth analyses of the indicated cell lines treated with the control and two independent METTL5 siRNAs. All cells were treated with first-round siRNA transfection for 3 days to ensure that METTL5 was significantly inhibited at protein level. All cells were then subjected to the second round of siRNA transfection (day 1 in the figure), and cells were harvested for MTS analyses at the indicated time points. Data are presented as mean ± SD; **$p < 0.01$.

(D) METTL5 knockdown led to reduced S6K phosphorylation (S6Kp) levels in the indicated breast cancer cell lines shown by western blotting.

Note that all experiments were repeated more than three times, and one replicate is shown.

lifespan and stress resistance, were observed in the worms treated with RNAi reagents targeting the transcripts of the ribosomal protein genes and S6K homolog *rsks-1* (Hansen et al., 2007), further supporting the conclusion that worm METL-5 also plays a conserved function in regulating protein translation.

The alterations in ribosome-mediated translational efficiency were coupled with the protein folding status (Zhang et al., 2009), so we next set out to determine the state of the unfolded protein response (UPR) in animals lacking *metl-5*. Interestingly, we found that the expression of *hsp-4p:gfp* (the UPR^{ER} reporter) was strongly induced in animals lacking *metl-5*, while the expression of the cytosolic UPR reporter *hsp-16.2p:gfp* or the mitochondrial UPR reporter *hsp-6p::gfp* was not affected in the *metl-5* mutants (Kim et al., 2016; Pellegrino et al., 2014; Ron and Walter, 2007; Roy and Lee, 1999; Tian et al., 2016; Yoneda et al., 2004) (Figures S5F–S5I). Consistently, the level of endogenous *hsp-4* (UPR^{ER} indicator) mRNA was also significantly upregulated in *metl-5* mutant animals compared with wild-type animals, but the mRNA levels of *hsp-6* (UPR^{mito} indicator) or *hsp-16.2* (UPR^{cyto} indicator) were not significantly changed (Figures S5J and S5K). Such observations indicated that the loss of METL-5 in worms could effectively induce UPR^{ER}, which was reported to affect stress responses and lifespan (Frakes and Dillin, 2017).

DISCUSSION

METTL5 Is a 18S rRNA A1832-Specific Methyltransferase

Although METTL5 was recently reported to be responsible for the 18S rRNA m^6A in multiple species (Chen et al., 2020; Ignatova et al., 2020; Leismann et al., 2020; Liberman et al., 2020; van Tran et al., 2019; Xing et al., 2020), substrate specificity and the requirement of substrate recognition were not investigated. Here, we showed that the recombinant METTL5 protein purified from insect Sf9 cells catalyzed m^6A modification on a 7 nt RNA probe with the 18S A1832 in the middle (GUAACAA), indicating that the primary substrate sequence is sufficient for the enzymatic recognition. However, at the endogenous 18S target, the 7 nt motif is embedded in a much longer transcript, so whether the flanking sequences and structural motifs are involved in regulating METTL5 activity is an interesting question to address in the future. Through database searches, we identified four mRNA transcripts containing GUAm^6ACAA sites, but none of them were dependent on METTL5 (Figure S1A), and no significant changes in m^6A abundance in the mRNA fraction were observed in METTL5-KO cells compared with controls (Figure 1F).

Importantly, we found that the recombinant METTL5 protein was inactive toward the AAACU, GAACU, and GGACU motifs (METTL3/14-preferred substrates) enriched in the m^6A modified mRNA species and the 28S rRNA m^6A motif UAACG (Figure 1A). Interestingly, both the METTL3/14 complex and the 28S m^6A methyltransferase ZCCHC4 were not active on the 18S probe (Figure 1D; Ma et al., 2019). Although these enzymes all contain the [D/N/S]PP/[F/Y] motif and thus function as m^6A methyltransferases, our results revealed that they have strong substrate specificities. Together with previous reports (Zhang et al., 2019; Ma et al., 2019; Pendleton et al., 2017), our findings indicate that the different m^6A events are individually regulated by unique pairs of the enzymes and substrate codes, similar to that of the histone lysine methylation network in which histone lysine methylations are believed to introduce both plasticity and complexity of transcription regulation. Here we hypothesize that the 18S rRNA m^6A1832 event is also evolved to fine-tune ribosome function and introduce translational plasticity in the response to environmental changes.

METTL5 Regulates Ribosome Function

Our data revealed significant defects in protein translation in METTL5-KO cells (Figures 3B and 3C). Such defects could be due to impaired translation initiation, reflected by significantly attenuated S6K activation, decreased amounts of 80S-associated EIF3A and EIF4E (Figures 3D, 3E, and 4D), and reduced polysome abundance, indicating that fewer ribosomes are at work (Figure 3A).

How a small methyl group at the ribosomal decoding center can initiate global effects on polysome profiling and translation initiation remains to be elucidated. The decoding center is composed of the h44 and h45 loops and is subjected to heavy rRNA modifications from prokaryotes to humans (Sergiev et al., 2018), leading us to hypothesize that these modifications may play fine-tuning roles in shaping decoding center conformation. We compared human 6OLE and yeast 6T7T structures and found that non-classical base pairing, m^6A1832-Cm1703, in the decoding center, might be affected by m^6A1832 methylation. Compared with the yeast and *E. coli* ribosomes, this base pairing is weakened in the human structure, and a clear movement of Cm1703 toward mRNA backbone was observed (Figures 2B–2D). The distance between the mRNA backbone and the N6 methyl group of human m^6A1832 is 5.6 Å, which is much closer compared with the unmethylated N6 nitrogen in yeast and *E. coli* (7.0 and 7.1 Å) (Figures 2B–2D). We expect that such differences may result in a conformation favoring stronger interaction between the human ribosome decoding center and mRNA by m^6A1832 and Cm1703.

As the ribosome is a very refined RNA-protein machinery, a series of structural changes in the decoding center caused by the loss of m^6A1832 may result in impaired decoding efficiency and rate, which may further affect the initiation step and 80S/polysome fractions to reduce the global translation (Figure 3). Whether our hypothesis of the structure changes is true will need future work to test. Nevertheless, the reporter assays using various 5′ cap and IRES reporters and protein content analyses demonstrated that the impact of METTL5 on translation is global (Figures 3C and S3A).

Another possibility could be that METTL5 also exert certain function through protein-protein interaction. Our IP-MS analyses not only confirmed the interaction between TRMT112 and METTL5 that was reported previously (Chen et al., 2020; Ignatova et al., 2020; Leismann et al., 2020; van Tran et al., 2019) but also uncovered many other interacting proteins that were significantly enriched in two functional groups (i.e., ribosome and translation related and RNA processing) (Figures S3B and S3C). Therefore, it is also possible that the METTL5 protein may act as an accessory factor in the assembly of an activated

ribosome with proper S6K phosphorylation signaling and EIF association through a protein-protein interacting mechanism.

Connection among METTL5, Growth Control, and Cancer

It is reported that protein translation activity is generally elevated in cancers, which require accelerated demand of nutrition to support the overgrowth (Pelletier et al., 2018; Robichaud et al., 2019). For instance, the biogenesis of ribosome, including ribosomal proteins and rRNAs, is significantly enhanced in certain cancers (Shi et al., 2017). Our study using breast cancer samples identified increased METTL5 expression in 7 of 10 cancer samples compared with their paratumor controls (Figure 4A). We further demonstrated that loss of METTL5 led to a reduced proliferation of several breast cancer cell lines, suggesting a role of METTL5 in breast cancer tumorigenesis. Consistently, we observed that the loss of METTL5 in many of the cell lines used in this study displayed reduced S6K phosphorylation, a signal that is connected to translation initiation and cell growth.

Interestingly, the reduced polysome and S6K phosphorylation have been previously reported in MCF7 cells treated with AMPK agonist or mTOR inhibitors (Dowling et al., 2007). Similar to our METL-5/*metl-5* mutant (Figures S5C and S5E), the S6K/*rsks-1* mutant worms also showed prolonged lifespan and thermotolerance (Hansen et al., 2007), and this longevity phenotype could be reversed by loss of *AMPK/aak-2* (Selman et al., 2009). It is unclear at this point whether METTL5 is under control of the AMPK or mTOR pathway and whether ribosomal activity is regulated in a similar way. Our worm studies suggest that the METL-5/*metl-5* phenotypes could be, at least in part, due to increased UPR^{ER}, which has been shown to be connected to nutrition/energy, translation status, stress resistance, and longevity (Frakes and Dillin, 2017). Future attempts should investigate whether METTL5 regulation of ribosome activity is integral for cellular energy and nutrition homeostasis. If so, METTL5 may serve as a potential therapeutic target for cancer and obesity and its small molecule inhibitor may achieve similar effect as constrained food intake and prolonged lifespan.

It is also worthy to note that previous attempts to target cancer by inhibiting the general translation machinery, such as S6K and EIF4A/4E/4E-BP phosphorylation, had been associated with toxicity issues, possibly due to side effects affecting normal cell survival. However, complete loss of METTL5 in certain human cells (HeLa in this study and HCT116 [van Tran et al., 2019]) and worms did not cause obvious cell death, indicating that targeting a ribosome modifier, such as METTL5, may bypass general toxicity issues and create therapeutic windows for inhibiting cancer cell growth.

The Biological Significance of METTL5: Adaptive Translation?

Previous studies support the concepts of specialized ribosome or ribosome heterogeneity (Ferretti and Karbstein, 2019; Shi and Barna, 2015; Shi et al., 2017). In general, variations in RP composition and ribosome modifications have been reported and associated with different growth conditions and developmental phenotypes (Shi and Barna, 2015). Our unpublished results in HEK293T cells and a recent study in mouse embryonic cells showed that the A1832 was 60%–70% methylated in the two cell lines (data not shown and Ignatova et al., 2020). Thus, the modification status of this site is heterogenic, at least in some culture cells.

Our worm findings were consistent with a very recently published study by Liberman et al. (2020), in which they demonstrated METL-5 as the 18S rRNA m^6A1717 methyltransferase in worms and found that the *metl-5* mutants showed enhanced stress resistance in response to heat, cold, and UV treatment. Although the authors found no evidence of global translation changes in the *metl-5* mutant strains, the translation of the *cyp-29A3* transcript was significantly affected, and the eicosanoid synthesis pathway was associated with the *metl-5* mutant phenotypes in their study. Compared with the study of Liberman et al. (2020), we have not yet identified the affected downstream mRNA molecules.

Loss of NSUN5, the 26S rRNA methylase mediating a conserved m^5C2278 modification close to the ribosome PTC (peptidyl transferase center) site, also led to extended lifespan and enhanced stress tolerance under the condition of limited food supply but not under the unstressed conditions (Schosserer et al., 2015). In our study, we observed that *metl-5* mutants developed extended lifespan under the unstressed conditions. Interestingly, NSUN5 loss also led to accumulated 80S and reduced polysome, again under stressed but not the unstressed condition. Here we saw that METTL5 loss resulted in similar changes in the polysome profile in the unstressed human cells (Figure 3A). These observations indicate that the two rRNA modifications may have certain intrinsic connections or overlapping functions in regulating ribosome to adapt the environmental changes. This is despite METTL5's appearing to have broader functions even under unstressed conditions. On a separate note, reduced NSUN5 expression level was reported to be associated with aging (Schosserer et al., 2015). Similarly, we also found significantly reduced expression of METTL5 in aged human tissues, including muscle, brain, blood, heart, colon, and lung (Figures S6A and S6B). Whether the reduced enzyme amount led to less modified ribosomes in the aged tissues, and if these are natural processes in place to respond to senescence-related stresses, are important questions that will require further investigations.

Recently, familiar recessive mutations in *METTL5* gene were reported in syndromic developmental disorders associated with intellectual disability and microcephaly (Richard et al., 2019). Some mutations were reported to cause METTL5 protein destabilization. Although it is unclear whether m^6A1832 levels in the patients were affected by these mutations, what is clear is that METTL5 is dispensable for major development but is required for refined organization and proper function of specific tissues. Again, all this evidence points to the same future direction of examining the regulation of METTL5 and m^6A1832 under different growth and stress conditions and in various biological models.

STAR★METHODS

Detailed methods are provided in the online version of this paper and include the following:

- KEY RESOURCES TABLE

- RESOURCE AVAILABILITY
  - Lead Contact
  - Materials Availability
  - Data and Code Availability
- EXPERIMENTAL MODEL AND SUBJECT DETAILS
  - Cell lines
  - Animals
  - Clinical Sample Acquisition
  - Recombinant proteins
- METHOD DETAILS
  - *In vitro* methyltransferase assay and HPLC analysis
  - Cell growth and cell cycle analysis
  - Immunofluorescence
  - BCA quantification of total protein
  - Isolation of rRNA fragments for HPLC analysis
  - mRNA isolation, m^6A-RIP and RT-qPCR
  - AHA Click labeling assay
  - Generation of METTL5 knockout cell lines by CRISPR-Cas9
  - Structure analyses
  - Polysome profiling
  - Dual Luciferase assays
  - *Caenorhabditis elegans* Maintenance and analyses
- QUANTIFICATION AND STATISTICAL ANALYSIS
  - GTEx gene expression data and analysis

SUPPLEMENTAL INFORMATION

Supplemental Information can be found online at https://doi.org/10.1016/j.celrep.2020.108544.

ACKNOWLEDGMENTS

We thank Dr. Renjing Liu for valuable advice during manuscript preparation. We thank Dr. Mark T. Bedford for the kind gift of the reporter constructs, and the National BioResource Project (NBRP) for supporting the *metl-5* mutant worm strains. This project was supported by the National Key Research and Development Program of China (2016YFA0101800 to F.L., 2018YFA0108700, and 2017YFA0506400 to Y.T.), the National Natural Science Foundation of China (31925010, 91953121, and 81773014 to F.L. and 31971330 to H.M.), the Shanghai Municipal Science and Technology Major Project (2017SHZDZX01), and the Strategic Priority Research Program of the Chinese Academy of Sciences (XDB39000000 to Y.T.).

AUTHOR CONTRIBUTIONS

B.R. carried out most of the experiments. Q.Z. performed worm work. J.W. conducted ribosome profiling. Q.Q. and W.Z. offered help in structure analyses. S.X. offered advice on cell growth experiment. Y.S. purified METTL3/METTL14 proteins. R.D., L.Z., and G.Y. performed MS analyses. Y.L. and J. Cai provided cancer samples. J.X. and H.G. performed the flow cytometry analysis. J.Chen and J.-D.J.H. performed aging-related analyses in human tissues. F.L., Y.T., and H.M. directed all the experiments and conceived the project.

DECLARATION OF INTERESTS

The authors declare no competing interests.

Received: April 21, 2020
Revised: September 3, 2020
Accepted: December 1, 2020
Published: December 22, 2020

REFERENCES

Behrmann, E., Loerke, J., Budkevich, T.V., Yamamoto, K., Schmidt, A., Penczek, P.A., Vos, M.R., Bürger, J., Mielke, T., Scheerer, P., and Spahn, C.M. (2015). Structural snapshots of actively translating human ribosomes. Cell *161*, 845–857.

Chandrasekaran, V., Juszkiewicz, S., Choi, J., Puglisi, J.D., Brown, A., Shao, S., Ramakrishnan, V., and Hegde, R.S. (2019). Mechanism of ribosome stalling during translation of a poly(A) tail. Nat. Struct. Mol. Biol. *26*, 1132–1140.

Chen, H., Liu, Q., Yu, D., Natchiar, K., Zhou, C., Hsu, C.-h., Hsu, P.-H., Zhang, X., Klaholz, B., Gregory, R.I., et al. (2020). METTL5, an 18S rRNA-specific m6A methyltransferase, modulates expression of stress response genes. bioRxiv. https://doi.org/10.1101/2020.04.27.064162.

Choi, Y.C., and Busch, H. (1978). Modified nucleotides in T1 RNase oligonucleotides of 18S ribosomal RNA of the Novikoff hepatoma. Biochemistry *17*, 2551–2560.

Coureux, P.D., Lazennec-Schurdevin, C., Bourcier, S., Mechulam, Y., and Schmitt, E. (2020). Cryo-EM study of an archaeal 30S initiation complex gives insights into evolution of translation initiation. Commun. Biol. *3*, 58.

Demirci, H., Murphy, F., 4th, Belardinelli, R., Kelley, A.C., Ramakrishnan, V., Gregory, S.T., Dahlberg, A.E., and Jogl, G. (2010). Modification of 16S ribosomal RNA by the KsgA methyltransferase restructures the 30S subunit to optimize ribosome function. RNA *16*, 2319–2324.

Dillin, A., Hsu, A.L., Arantes-Oliveira, N., Lehrer-Graiwer, J., Hsin, H., Fraser, A.G., Kamath, R.S., Ahringer, J., and Kenyon, C. (2002). Rates of behavior and aging specified by mitochondrial function during development. Science *298*, 2398–2401.

Dowling, R.J., Zakikhani, M., Fantus, I.G., Pollak, M., and Sonenberg, N. (2007). Metformin inhibits mammalian target of rapamycin-dependent translation initiation in breast cancer cells. Cancer Res. *67*, 10804–10812.

Doxtader, K.A., Wang, P., Scarborough, A.M., Seo, D., Conrad, N.K., and Nam, Y. (2018). Structural basis for regulation of METTL16, an S-adenosylmethionine homeostasis factor. Mol. Cell *71*, 1001–1011.e4.

Ferretti, M.B., and Karbstein, K. (2019). Does functional specialization of ribosomes really exist? RNA *25*, 521–538.

Fischer, N., Neumann, P., Konevega, A.L., Bock, L.V., Ficner, R., Rodnina, M.V., and Stark, H. (2015). Structure of the E. coli ribosome-EF-Tu complex at <3 Å resolution by Cs-corrected cryo-EM. Nature *520*, 567–570.

Frakes, A.E., and Dillin, A. (2017). The UPR^{ER}: sensor and coordinator of organismal homeostasis. Mol. Cell *66*, 761–771.

Győrffy, B., Lanczky, A., Eklund, A.C., Denkert, C., Budczies, J., Li, Q., and Szallasi, Z. (2010). An online survival analysis tool to rapidly assess the effect of 22,277 genes on breast cancer prognosis using microarray data of 1,809 patients. Breast Cancer Res. Treat. *123*, 725–731.

Hansen, M., Taubert, S., Crawford, D., Libina, N., Lee, S.J., and Kenyon, C. (2007). Lifespan extension by conditions that inhibit translation in Caenorhabditis elegans. Aging Cell *6*, 95–110.

Ignatova, V.V., Stolz, P., Kaiser, S., Gustafsson, T.H., Lastres, P.R., Sanz-Moreno, A., Cho, Y.L., Amarie, O.V., Aguilar-Pimentel, A., Klein-Rodewald, T., et al. (2020). The rRNA m^6A methyltransferase METTL5 is involved in pluripotency and developmental programs. Genes Dev. *34*, 715–729.

Khatter, H., Myasnikov, A.G., Natchiar, S.K., and Klaholz, B.P. (2015). Structure of the human 80S ribosome. Nature *520*, 640–645.

Kim, H.E., Grant, A.R., Simic, M.S., Kohnz, R.A., Nomura, D.K., Durieux, J., Riera, C.E., Sanchez, M., Kapernick, E., Wolff, S., et al. (2016). Lipid biosynthesis coordinates a mitochondrial-to-cytosolic stress response. Cell *166*, 1539–1552.e16.

Kimura, S., and Suzuki, T. (2010). Fine-tuning of the ribosomal decoding center by conserved methyl-modifications in the Escherichia coli 16S rRNA. Nucleic Acids Res. *38*, 1341–1352.

Leismann, J., Spagnuolo, M., Pradhan, M., Wacheul, L., Vu, M.A., Musheev, M., Mier, P., Andrade-Navarro, M.A., Graille, M., Niehrs, C., et al. (2020). The

18S ribosomal RNA m^6 A methyltransferase Mettl5 is required for normal walking behavior in Drosophila. EMBO Rep. *21*, e49443.

Li, W., Ward, F.R., McClure, K.F., Chang, S.T., Montabana, E., Liras, S., Dullea, R.G., and Cate, J.H.D. (2019). Structural basis for selective stalling of human ribosome nascent chain complexes by a drug-like molecule. Nat. Struct. Mol. Biol. *26*, 501–509.

Liberman, N., O'Brown, Z.K., Earl, A.S., Boulias, K., Gerashchenko, M.V., Wang, S.Y., Fritsche, C., Fady, P.E., Dong, A., Gladyshev, V.N., and Greer, E.L. (2020). N6-adenosine methylation of ribosomal RNA affects lipid oxidation and stress resistance. Sci. Adv. *6*, eaaz4370.

Linder, B., Grozhik, A., Olarerin-George, G., et al. (2015). Single-nucleotide-resolution mapping of m6A and m6Am throughout the transcriptome. Nat. Methods *12*, 767–772.

Ma, H., Wang, X., Cai, J., Dai, Q., Natchiar, S.K., Lv, R., Chen, K., Lu, Z., Chen, H., Shi, Y.G., et al. (2019). N^{6-}Methyladenosine methyltransferase ZCCHC4 mediates ribosomal RNA methylation. Nat. Chem. Biol. *15*, 88–94.

Maden, B.E.H. (1986). Identification of the locations of the methyl groups in 18 S ribosomal RNA from Xenopus laevis and man. J. Mol. Biol. *189*, 681–699.

Natchiar, S.K., Myasnikov, A.G., Kratzat, H., Hazemann, I., and Klaholz, B.P. (2017). Visualization of chemical modifications in the human 80S ribosome structure. Nature *551*, 472–477.

Nürenberg-Goloub, E., Kratzat, H., Heinemann, H., Heuer, A., Kötter, P., Berninghausen, O., Becker, T., Tampé, R., and Beckmann, R. (2020). Molecular analysis of the ribosome recycling factor ABCE1 bound to the 30S post-splitting complex. EMBO J. *39*, e103788.

Pellegrino, M.W., Nargund, A.M., Kirienko, N.V., Gillis, R., Fiorese, C.J., and Haynes, C.M. (2014). Mitochondrial UPR-regulated innate immunity provides resistance to pathogen infection. Nature *516*, 414–417.

Pelletier, J., Thomas, G., and Volarević, S. (2018). Ribosome biogenesis in cancer: new players and therapeutic avenues. Nat. Rev. Cancer *18*, 51–63.

Pendleton, K.E., Chen, B., Liu, K., Hunter, O.V., Xie, Y., Tu, B.P., and Conrad, N.K. (2017). The U6 snRNA m(6)A methyltransferase METTL16 regulates SAM synthetase intron retention. Cell *169*, 824–835.e14.

Poldermans, B., Roza, L., and Van Knippenberg, P.H. (1979). Studies on the function of two adjacent N6,N6-dimethyladenosines near the 3′ end of 16 S ribosomal RNA of Escherichia coli. III. Purification and properties of the methylating enzyme and methylase-30 S interactions. J. Biol. Chem. *254*, 9094–9100.

Richard, E.M., Polla, D.L., Assir, M.Z., Contreras, M., Shahzad, M., Khan, A.A., Razzaq, A., Akram, J., Tarar, M.N., Blanpied, T.A., et al. (2019). Bi-allelic variants in METTL5 cause autosomal-recessive intellectual disability and microcephaly. Am. J. Hum. Genet. *105*, 869–878.

Robichaud, N., Sonenberg, N., Ruggero, D., and Schneider, R.J. (2019). Translational control in cancer. Cold Spring Harb. Perspect. Biol. *11*, a032896.

Ron, D., and Walter, P. (2007). Signal integration in the endoplasmic reticulum unfolded protein response. Nat. Rev. Mol. Cell Biol. *8*, 519–529.

Roy, B., and Lee, A.S. (1999). The mammalian endoplasmic reticulum stress response element consists of an evolutionarily conserved tripartite structure and interacts with a novel stress-inducible complex. Nucleic Acids Res. *27*, 1437–1443.

Schosserer, M., Minois, N., Angerer, T.B., Amring, M., Dellago, H., Harreither, E., Calle-Perez, A., Pircher, A., Gerstl, M.P., Pfeifenberger, S., et al. (2015). Methylation of ribosomal RNA by NSUN5 is a conserved mechanism modulating organismal lifespan. Nat. Commun. *6*, 6158.

Selman, C., Tullet, J.M., Wieser, D., Irvine, E., Lingard, S.J., Choudhury, A.I., Claret, M., Al-Qassab, H., Carmignac, D., Ramadani, F., et al. (2009). Ribosomal protein S6 kinase 1 signaling regulates mammalian life span. Science *326*, 140–144.

Sergiev, P.V., Aleksashin, N.A., Chugunova, A.A., Polikanov, Y.S., and Dontsova, O.A. (2018). Structural and evolutionary insights into ribosomal RNA methylation. Nat. Chem. Biol. *14*, 226–235.

Shao, S., Murray, J., Brown, A., Taunton, J., Ramakrishnan, V., and Hegde, R.S. (2016). Decoding mammalian ribosome-mRNA states by translational GTPase complexes. Cell *167*, 1229–1240.e15.

Shi, Z., and Barna, M. (2015). Translating the genome in time and space: specialized ribosomes, RNA regulons, and RNA-binding proteins. Annu. Rev. Cell Dev. Biol. *31*, 31–54.

Shi, Z., Fujii, K., Kovary, K.M., Genuth, N.R., Rost, H.L., Teruel, M.N., and Barna, M. (2017). Heterogeneous ribosomes preferentially translate distinct subpools of mRNAs genome-wide. Mol. Cell *67*, 71–83.e7.

Shi, H., Wei, J., and He, C. (2019). Where, when, and how: context-dependent functions of RNA methylation writers, readers, and erasers. Mol. Cell *74*, 640–650.

Tesina, P., Lessen, L.N., Buschauer, R., Cheng, J., Wu, C.C., Berninghausen, O., Buskirk, A.R., Becker, T., Beckmann, R., and Green, R. (2020). Molecular mechanism of translational stalling by inhibitory codon combinations and poly(A) tracts. EMBO J. *39*, e103365.

Tian, Y., Garcia, G., Bian, Q., Steffen, K.K., Joe, L., Wolff, S., Meyer, B.J., and Dillin, A. (2016). Mitochondrial stress induces chromatin reorganization to promote longevity and UPR(mt). Cell *165*, 1197–1208.

van Tran, N., Ernst, F.G.M., Hawley, B.R., Zorbas, C., Ulryck, N., Hackert, P., Bohnsack, K.E., Bohnsack, M.T., Jaffrey, S.R., Graille, M., and Lafontaine, D.L.J. (2019). The human 18S rRNA m6A methyltransferase METTL5 is stabilized by TRMT112. Nucleic Acids Res. *47*, 7719–7733.

Wang, L., Liang, Y., Lin, R., et al. (2020). Mettl5 mediated 18S rRNA N6-methyladenosine (m6A) modification controls stem cell fate determination and neural function. Genes & Diseases, Published online July 17, 2020. https://doi.org/10.1016/j.gendis.2020.07.004.

Xing, M., Liu, Q., Mao, C., Zeng, H., Zhang, X., Zhao, S., Chen, L., Liu, M., Shen, B., Guo, X., et al. (2020). The 18S rRNA m^6 A methyltransferase METTL5 promotes mouse embryonic stem cell differentiation. EMBO Rep. *21*, e49863.

Xu, Z., O'Farrell, H.C., Rife, J.P., and Culver, G.M. (2008). A conserved rRNA methyltransferase regulates ribosome biogenesis. Nat. Struct. Mol. Biol. *15*, 534–536.

Yoneda, T., Benedetti, C., Urano, F., Clark, S.G., Harding, H.P., and Ron, D. (2004). Compartment-specific perturbation of protein handling activates genes encoding mitochondrial chaperones. J. Cell Sci. *117*, 4055–4066.

Zhang, G., Hubalewska, M., and Ignatova, Z. (2009). Transient ribosomal attenuation coordinates protein synthesis and co-translational folding. Nat. Struct. Mol. Biol. *16*, 274–280.

Zhang, Z., Chen, L.Q., Zhao, Y.L., Yang, C.G., Roundtree, I.A., Zhang, Z., Ren, J., Xie, W., He, C., and Luo, G.Z. (2019). Single-base mapping of m^6A by an antibody-independent method. Sci. Adv. *5*, eaax0250.

Zorbas, C., Nicolas, E., Wacheul, L., Huvelle, E., Heurgué-Hamard, V., and Lafontaine, D.L. (2015). The human 18S rRNA base methyltransferases DIMT1L and WBSCR22-TRMT112 but not rRNA modification are required for ribosome biogenesis. Mol. Biol. Cell *26*, 2080–2095.

STAR★METHODS

KEY RESOURCES TABLE

REAGENT or RESOURCE	SOURCE	IDENTIFIER
Antibodies		
Rabbit Anti-Human METTL5 Polyclonal Antibody	Proteintech	Cat# 16791-1-AP; RRID:AB_2142051
HRP-Conjugated Alpha Tubulin Antibody	Proteintech	Cat# HRP-66031; RRID:AB_2687491
Lamin B1 Antibody	Proteintech	Cat# 66095-1-Ig; RRID:AB_2721256
Rabbit Anti-Human RPS6 Polyclonal Antibody	Proteintech	Cat# 14823-1-AP; RRID:AB_2181025
RPL4 antibody	Proteintech	Cat# 11302-1-AP; RRID:AB_2181909
HRP-conjugated streptavidin	Proteintech	Cat# SA00001-0
Phospho-p70 S6 Kinase (Thr389) Antibody	Cell Signaling Technology	Cat# 9205; RRID:AB_330944
p70 S6 Kinase Antibody	Cell Signaling Technology	Cat# 9202; RRID:AB_2269804
eIF3A (D51F4) XP Rabbit mAb antibody	Cell Signaling Technology	Cat# 3411; RRID:AB_2096523
eIF4E (C46H6) Rabbit mAb antibody	Cell Signaling Technology	Cat# 2067; RRID:AB_2097675
Goat anti-Rabbit IgG Secondary Antibody HRP-labled	Signalway	Cat# L3012; RRID:AB_895483
Goat anti-Mouse IgG Secondary Antibody HRP-labled	Signalway	Cat# L3032; RRID:AB_895481
Mouse Anti-beta-Actin Monoclonal Antibody	Sigma-Aldrich	Cat# A5441; RRID:AB_476744
m6A-202 003	Synaptic Systems	Cat# 202003; RRID:AB_2279214
Bacterial and Virus Strains		
Top10 Competent Cells	SMART-Lifesciences	Cat# SLB010
DH10Bac Competent Cells	Our Lab	N/A
Biological Samples		
primary breast tissue obtained from patients	Fudan University Shanghai Cancer Center	N/A
Chemicals, Peptides, and Recombinant Proteins		
Nuclease P1	Wako	Cat# 145-08221
FastAP	Thermo scientific	Cat# EF0651
Magnetic Oligo d(T)25 beads	NEB	Cat# S1419S
TRIzol	Thermo scientific	Cat# 15596018
DynabeadsTM MyOneTM Streptavidin T1	Invitrogen	Cat# 65602
RNaseA	Thermo scientific	Cat# EN0531
Mung bean nuclease	NEB	Cat# M0250S
cycloheximide	MCE	Cat# HY-12320
SUPERase inhibitor	Thermo scientific	Cat# AM2694
Biotin-Alkyne	SIGMA	Cat# 764213-5MG
TCEP	Invitrogen	Cat# 20490
Sucrose	VWR Lifesciences	Cat# M117-500G
CuSO4	Sinopharm	Cat# 89101810-1
THPTA	SIGMA	Cat# 762342-100MG
FUDR	Aladdin	Cat# F110732
Lipofectamine 2000 Transfection Reagent	Thermo scientific	Cat# 11668019
Lipofectamine RNAiMAX Transfection Reagent	Thermo scientific	Cat# 13778150

(*Continued on next page*)

Continued

REAGENT or RESOURCE	SOURCE	IDENTIFIER
PrimeScript RT Reagent Kit	Takara	Cat# RR047A
FastStart Universal SYBR Green master (Rox)	Roche	Cat# 4913914001
Cellfectin II Reagent	Thermo scientific	Cat# 10362100
Critical Commercial Assays		
CellTiter 96 AQueous one solution	Promega	Cat# G3581
cell cycle analysis kit	Beyotime	Cat# C1052
Annexin V-FITC apoptosis detection kit	Beyotime	Cat# C1062L
Dual Luciferase reporter gene assay kit	Beyotime	Cat# RG027
RiboMinus Eukaryote kit v2	Ambion	Cat# A15020
Experimental Models: Cell Lines		
Human: HEK293T	ATCC	Cat# CRL-3216
Human: HeLa	ATCC	Cat# CCL-2
Human: MCF7	ATCC	Cat# HTB-22
Human: T47D	ATCC	Cat# HTB-133
Human: MDA-MB-231	ATCC	Cat# HTB-26
Human: ZR75-30	ATCC	Cat# CRL-1504
Sf9 Insect cells	ATCC	Cat# CRL-1711
Experimental Models: Organisms/Strains		
C. elegans: N2	CGC	WormBase ID: N2
C. elegans: metl-5(tm4476)	NBRP	N/A
C. elegans: metl-5(tm4561)	NBRP	N/A
Oligonucleotides		
See Table S1		N/A
Recombinant DNA		
modified pFastbac vector	This paper	N/A
pX459-METTL5 KO1	This paper	N/A
pX459-METTL5 KO2	This paper	N/A
pRF-reporter	Mark T. Bedford Lab	N/A
pRF-HCV	Mark T. Bedford Lab	N/A
pRF-CCND1	Mark T. Bedford Lab	N/A
pRF-ESR1	Mark T. Bedford Lab	N/A
pRF-HIF1a	Mark T. Bedford Lab	N/A
pRF-cMYC	Mark T. Bedford Lab	N/A
Software and Algorithms		
PyMOL 3D structure viewer	Schrödinger	https://pymolwiki.org/
FlowJo	BDbiosciences	https://www.flowjo.com/
Graphpad	GraphPad	https://www.graphpad.com/

RESOURCE AVAILABILITY

Lead Contact

Further information and requests for resources and reagents may be directed to and will be fulfilled by the Lead Contact, Fei Lan (fei_lan@fudan.edu.cn)

Materials Availability

All unique/stable reagents generated in this study are available from the Lead Contact with a completed Materials Transfer Agreement.

Data and Code Availability

This study did not generate any unique datasets or code.

EXPERIMENTAL MODEL AND SUBJECT DETAILS

Cell lines

Human HEK293T, HeLa, MCF7, MDA-MB-231, T47D and ZR75-30 cell lines were used for experiments. All cells were cultured in DMEM (HyClone, Cat No. SH30243.01), supplemented with 10% fetal bovine serum (Biological Industries, 04-001-1ACS) and 1% Penicillin-Streptomycin (HyClone, SV30010.01) at 37°C and under 5% CO_2.

Animals

metl-5 mutant worm strains were supported by NBRP. *C. elegans* strains were maintained at 20°C on standard nematode growth medium agar (NGM) plates seeded with *Escherichia coli* OP50 bacteria unless otherwise stated.

Clinical Sample Acquisition

A total of 10 paired tumor, adjacent non-tumor breast tissues were obtained from a cohort of patients undergoing surgery at Fudan University Shanghai Cancer Center. Tissue samples were collected within 30 min after operation and snap-frozen in liquid nitrogen before use. For protein extraction, frozen tissues (20 mg) were grinded thoroughly into fine powder in liquid nitrogen using a pestle, and then 200 μL SDS lysis buffer was added per sample. The protein samples were then denatured at 95°C for 5 min before SDS-PAGE examination, and then quantified by Coomassie Brilliant Blue staining. For western blotting analyses in Figure 4A, equal amount protein samples (around 20 μg) were used. The study was approved by the FUSCC Ethics Committee and written informed consent was obtained from each patient.

Recombinant proteins

C-terminal Flag-tagged METTL5 plasmid was constructed with a modified pFastBac vector using BamHI and XhoI sites for expression in baculovirus system. 48 hours after SF9 cells was infected by the viruses, cell pellets were lysed in lysis buffer containing 25 mM Tris-HCl pH 7.5, 300 mM NaCl, 0.1% Triton X-100, 1 mM PMSF and 1 x Protease Inhibitor Cocktail. Total lysate was incubated with anti-Flag affinity gel beads (SMART life-sciences, SA042005) for 3-4 hours, and washed twice with lysis buffer. Then recombinant Flag-METTL5 protein was eluted with elution buffer containing 25 mM Tris-HCl pH 7.5, 300 mM NaCl and 200 μg/ml Flag peptide.

METHOD DETAILS

In vitro methyltransferase assay and HPLC analysis

RNA probes containing the indicated motifs in Figure 1 were synthesized with 3′ biotinylation for further purification after methyltransferase assay (also see Table S1).

AAACU probe: 5′-GUCGUAAACUGGCUC-3′Biotin;
GAACU probe: 5′-GUCGUGAACUGGCUC-3′Biotin;
GGACU probe: 5′-GUCGUGGACUGGCUC-3′Biotin;
UAACG probe: 5′-CGGUAACGCAGGUGU-3′Biotin;
UAACA probe: 5′-AGUCGUAACAAGGUUUCCG-3′Biotin;
UAGCA probe: 5′-AGUCGUAGCAAGGUUUCCG-3′Biotin;
UAACA 15nt probe: 5′-AGUCGUAACAAGGUU-3′Biotin;
UAACA 11nt probe: 5′-UCGUAACAAGG-3′Biotin;
UAACA 7nt probe: 5′-GUAACAA-3′Biotin;
UAACA 5nt probe: 5′-UAACA-3′Biotin.

In vitro methyltransferase assay was performed in a 20 μL of reaction mixture containing 4 μg RNA probes, 5 μg recombinant protein, 0.1 mM SAM, 50 mM Tris-HCl pH 8.0, 5 mM $MgCl_2$, 1 mM DTT. The mixture was incubated in 16°C overnight. After incubation, samples were incubated with Dynabeads™ MyOne™ Streptavidin T1 beads at 4°C for 2 hours. Then beads were washed twice with binding buffer (50 mM Tris-HCl pH 7.5, 150 mM NaCl, 0.1% NP40) and DEPC H_2O separately. The desalinated RNA was then digested with nuclease P1 (Wako, 145-08221) and alkaline phosphatase (Thermo scientific, EF0652). Nucleosides were quantified by HPLC-MS/MS at MS facility of Fudan IBS institute.

Cell growth and cell cycle analysis

For growth analyses, 3000 cells per well were seeded in 96-well plate and measured by MTS (Promega, CellTiter 96 AQueous one solution) after two rounds of transfection. siRNAs were used to knockdown METTL5 in breast cancer cell lines, and the sequences are listed below.

siRNA1: 5′-AAGGAACUAGAGAGUCGCCUG-3′;
siRNA2: 5′-AUCCUACCAGGCCGCACAUUG-3′;
Negative control: 5′-UUCUCCGAACGUGUCACG-3′.

Cell cycle analyses were performed according to manufacturer's instruction (Beyotime C1052), and the apoptotic cells were detected using Annexin V-FITC kit (Beyotime C1062L) followed by flow cytometry analyses (BD FACSCanto).

Immunofluorescence

HEK293T cells overexpressing METTL5-Flag were detected by our homemade Flag antibody and Alexa Fluor 488 labeled goat anti mouse IgG (H+L) secondary antibody (Beyotime, A0428). DNA was stained by DAPI (Beyotime, C1002) and the signals were detected by Olympus FV1200.

BCA quantification of total protein

Total protein quantification was performed according to manufacturer's instruction (Beyotime P0011). In brief, equal amount of WT and METTL5-KO HeLa cells were collected and lysated in 2% SDS, and then heated under 95°C, then equal volume of cell lysis was added into the reaction buffer and incubated in 37°C for 1 hour, followed by A562 absorbance detection and analysis (Bio Tek Gen5).

Isolation of rRNA fragments for HPLC analysis

Isolation of the m^6A containing regions in 18S and 28S (or 26S in worm) rRNAs was carried out as previously described (Ma et al., 2019). In brief, we synthesized oligo DNA probes complementary to U1821-A1860 nucleotides of the human 18S and G4201-G4240 of the human 28S rRNA with 5′biotin.

Homo-18S probe:
5′-Biotin-TTCCGCAGGTTCACCTACGGAAACCTTGTTACGACTTTTA-3′
Homo-28S probe:
5′-Biotin-CTCGCCTTAGGACACCTGCGTTACCGTTTGACAGGTGTAC-3′
The corresponding worm oligo DNA probes are:
C.elegans-18S probe:
5′-Biotin-AGCTGCAGGTTCACCTACAGCTACCTTGTTACGACTTTTA-3′
C.elegans-26S probe:
5′-Biotin-CTCGCCTTAGGACACCTACGTTACGATTTGATAGATGTAC-3′

Total RNA was isolated by Trizol reagent, and 30 μg total RNA were then incubated with 5 μg DNA probe in the hybridization buffer containing 250 mM HEPES pH 7.0 and 500 mM KCl and treated with a standard denaturing and annealing protocol. After Mung bean nuclease and RNaseA digestion at 37°C for 1 hour, the hybridized 40 nt RNA fragments containing m^6A site of 18S rRNA and 28S rRNA were isolated from examined cells, and then the annealed fragments were incubated with DynabeadsTM MyOneTM Streptavidin T1 beads at 4°C for 1 hour. After washing, beads were heated at 70°C to isolate RNA fragments and then the RNA fragments were digested with nuclease P1 and alkaline phosphatase followed by HPLC analysis at MS facility of Fudan IBS institute.

mRNA isolation, m^6A-RIP and RT-qPCR

Total RNA was isolated by Trizol reagent, and 100 μg total RNA was used to isolate mRNA per analysis. Magnetic Oligo d(T)25 beads (NEB) and RiboMinus Eukaryote kit v2 (Ambion) were used to isolate mRNA and to remove contaminant rRNA respectively. The isolated polyA RNA was concentrated and measured with nanodrop. A total of 200 ng polyA RNA was digested with Nuclease P1 and alkaline phosphatase followed by HPLC analyses at MS facility of Fudan IBS institute.

For mRNA m^6A-RIP experiment, a total of 2 μg mRNA per sample was used. In brief, mRNA samples were first fragmented to around 200 nt by sonication, and 1% of the fragmented RNA samples were saved as input, and the rest were incubated with 5 μg m^6A antibody per IP reaction overnight in the IP buffer (10 mM Tris-HCl, pH 7.4, 150 mM NaCl, 0.1% NP-40, SUPERaseIn inhibitor in RNase-free water), followed by immobilizing on pre-washed protein A beads (20 μL per reaction) for 2 hours, and then the beads were washed with IP buffer for three times. The m^6A containing RNA samples were isolated using TRIzol method and then reverse transcribed to cDNA using PRImeScript RT Reagent Kit (Takara) according to the manufacturer's protocol. Quantitative PCR (qPCR) was performed using FastStart Universal SYBR Green master (Rox) (Roche). Primers used for RIP-qPCR were listed in Table S1.

AHA Click labeling assay

A total of 4×10^5 cells were seeded into one well of a 6-well plate and the medium was changed to DMEM without methionine (GIBCO, 21013-024) for 1 hour, and then supplemented with 10 mM AHA (L-Azidohomoalanine) for 3 hours. After twice washs with cold PBS, cells were lysed in lysis buffer (50 mM Tris-HCl pH 8.0 and 1% SDS), followed by sonication for 2 min. Cell debris were cleared by 13,000 rpm for 10 min, and protein concentrations were determined by A280. Equal amount of protein extracts (less than 2 μg/μl) were used for each reaction. The protein extracts were incubated with 100 μM Biotin-Alkyne 1 mM TCEP, 100 μM

THPTA and 1 mM CuSO4, and each addition was followed by short vortex for several seconds, and the mixtures were rotated at 25°C for 1 hour, and then precipitated by methanol precipitation. Equal volumes of lysates were analyzed by SDS-PAGE separation, and measured by HRP-conjugated streptavidin (proteintech, SA00001-0) with a standard western blotting protocol.

Generation of METTL5 knockout cell lines by CRISPR-Cas9

METTL5-KO cells were generated using a CRISPR-Cas9 approach. Two sgRNAs targeting METTL5 exon2 (5′-GCCGCCC TACCTGCAATGTG-3′) and exon3 (5′- AGCATCGGAACTGCAATGTT-3′) were cloned into pX459 respectively (see Table S1). The sgRNA plasmids were transfected into HEK293T or HeLa cells with Lipofectamine 2000, followed by puromycin selection for 48 hours, and then single clones were obtained by limited dilution. METTL5-KO cells were detected by western blotting using a specific antibody.

Structure analyses

The structure models and primary maps of the indicated ribosomes were downloaded from Protein Data Bank (PDB) and EMData Resource websites. Structures were edited using PyMOL and the maps were visualized by Wincoot. The PDB and EMD numbers of the structures used in this paper are 4UG0 (EMD_2938), 5AJ0 (EMD_2875), 6OLE (EMD_0600), 5LZS (EMD_4130), 6SGC (EMD_10181), 6T7T (EMD_10397) and 5AFI (EMD_2847).

Polysome profiling

In brief, two 10 cm dish of HEK293T or HeLa cells at 50% confluence were treated with cycloheximide (CHX) at 100 μg/ml for 2-10 min before collection. Cells were washed twice with cold PBS supplemented with 100 μg/ml CHX, scraped and pelleted by centrifugation at 1,000 rpm for 3 min at 4°C. Cell pellets were resuspended in 500 μL lysis buffer (25 mM Tris-HCl pH 7.5, 150 mM NaCl, 15 mM $MgCl_2$, 1 mM DTT, 8% Glycerol, 1% Triton X-100, 0.5% Na-Deoxycholate, 100 μg/ml CHX, 100 U/ml SUPERase inhibitor, 1 x Protease Inhibitor Cocktail), and debris and nuclei were cleared by centrifugation at 12,500 rpm for 10min. RNA concentration was determined by A260 using nanodrop (Thermo) and 7.5 OD of lysates were loaded on 10% - 50% sucrose gradients. Gradients were centrifuged on a SW40Ti rotor (Beckman Coulter) for 3.5 hours at 36,000 rpm at 4°C. Samples were fractioned and measured by an UV monitor and fraction collector. Proteins were obtained by methanol precipitation and analyzed by western blotting.

Dual Luciferase assays

A total of 5 × 10^5 HEK293T WT and METTL5-KO cells were seeded in one well of a 6-well plate. pRF reporter plasmid and other 5 IRES containing reporter plasmids, 1 μg for each, were transfected into cells using Lipofectamine 2000, and cultured for 48 hours. Luciferase activities were measured using dual luciferase reporter gene assay kit (Beyotime, RG027) to obtain firefly and renilla luminescences with at least 3 replicates.

Caenorhabditis elegans Maintenance and analyses

For Heat shock resistance assay, synchronized Day 1 worms were incubated at 34°C for 6 hours, and then recovered at 20°C for 8 hours before analyzing the survival rate. Experiments were performed using 6 plates with more than 20 animals in each.

Lifespan analyses were performed at 20°C as previously described (Dillin et al., 2002). Briefly, the assays were performed on *E. coli* OP50 and transfer to plates with FUDR (200 μL10 mg/mL) at L4 stage. Graphpad Prism 6 software was used for statistical analyses, and the Log-rank (Mantel-Cox) method was used to determine the level of significance.

For Developmental rate analyses, worms were synchronized and 200 eggs of each strain were placed onto each NGM plates with seeded OP50. The worms grew at 20°C for 60 hours and the number of worms at each developmental stage was calculated.

For imaging Analyses, micrographs of whole-worm images were acquired using a Leica M165 FC dissecting microscope and LAS X software. About 10 worms were anesthetized using sodium azide (50 mM). Exposure times were the same within each experiment. All animals used for images were day 2 adult hermaphrodites. All images are representative of more than three images. To quantify the intensity of GFP fluorescence, the entire region of the intestine was outlined and analyzed using ImageJ software.

QUANTIFICATION AND STATISTICAL ANALYSIS

For *in vitro* enzyme activity in Figures 1A–1D, all experiments were repeated three times, and one replicate was shown. For LC-MS/MS detected m^6A/A or m^6A/G level, data for Figures 1E and S5B, experiments were performed three times, and one replicate was shown. P values were determined using two-tailed Student's unpaired t test for the reporter assay (Figure 3C), protein quantification (Figure S3A), breast cancer cells proliferation (Figure 4C; Figure S4C) and RIP-qPCR (Figure S1A). For worm studies in Figure S5, each was repeated three times independently. Statistical analysis was carried out using Graphpad Prism 6 software, and all data presented as means ± s.d., *** $p < 0.001$, ** $p < 0.01$, * $p < 0.05$, n.s., non-significant. Statistical analyses information can also be found in each figure legend.

GTEx gene expression data and analysis

For the analysis of METTL5 expression levels in aged human tissues in Figure S6, the gene TPM data were obtained from the GTEx Portal and dbGaP accession number phs000424.v8.p2. Meta data were obtained from phs000424.v8.pht002742.v8.p2.c1.GTEx_Subject_Phenotypes.GRU.txt. For each tissue with more than 20 samples (27 tissues altogether), linear regression analyses and significance tests of METTL5 expression to age in males and females were obtained by l m (Expression∼Age) and the type II sum of squares was calculated using the ANOVA function of the R car package. This sum of squares type tests for each main effect after the other main effects. Multiple testing BH corrected FDR of the t test p values and linear regression p values were obtained by p.adjust (pvalues, method = ''fdr'') in R based on all 27 tested tissues. The scatterplots were plotted by R package ''ggplot2.''